Experiments in Fluids 29 (2000) 215–227 © Springer-Verlag 2000

Rotating cylinder drag balance with application to riblets

T. Hall, D. Joseph

Abstract Experimental results are reported and discussed for a rotating cylinder drag balance designed to predict drag reduction by surfaces like riblets. The apparatus functions by measuring the torque applied to the inner cylinder by a fluid, such as water, that is set in motion by the controlled rotation of the outer cylinder. The instrument was validated by calibration for laminar flow and comparison of turbulent flow results to the those of G. I. Taylor. The ability to predict drag reduction was demonstrated by testing 114 μm symmetric sawtooth riblets, which gave a maximum reduction of about 5% and an overall drag reduction range of $5 < S^+ < 20$, both of which are in excellent comparison to results reported in literature. The most suitable conditions for testing riblets are to apply the riblets only to the inner cylinder surface and to use cylinders for which the curvature of the flow is minimized.

1 Introduction

Skin friction drag has been a topic of great interest in the research community for some time now, largely because of its relevance to applications such as air flight, underwater travel, and high speed transport through pipes (e.g. water flowing through a fire hose). Any reduction in this drag can lead to significant energy savings for the industries associated with these applications, and thus an extensive effort has been made over recent decades to develop methods for achieving this goal. One of the more successful drag reducing methods conceived from this work has been riblets, i.e. stream-wise grooves along the drag-inflicted surface which restrict the turbulence intensity in the span-wise direction.

Many experimental studies have been conducted to study riblet surfaces and optimize the size and shape of the riblets to obtain the greatest possible reduction in drag. Most, if not all, of this work has been done in either a windtunnel or fluid channel, both of which are quite suitable for such testing but are also relatively large-scale and costly experimental facilities. Issues such as securing use of the facility, developing and implementing a method of representing the riblets on the desired surface, and finding a shear stress balance with sufficient accuracy all contribute to the cost of performing such tests. The time necessary to complete the tests can be augmented by pre-test preparation, such as manufacturing the riblet surface and affixing it to the test platform, and by the "turn-over" time for testing different riblet surfaces. From an industrial perspective, it may be too risky for a small company looking to develop similar technology to do so in a large-scale facility if they are not willing to absorb the cost in the event that the test results are not favorable.

The focus of the present investigation was to simplify this process by developing a small-scale experimental instrument for measuring the drag on surfaces like (but not limited to) riblets with acceptable accuracy but low cost and high efficiency. Such an instrument is the rotating cylinder drag balance described herein, which employs rotating shear flow between concentric cylinders to produce a measurable stress on the surfaces within the gap. The outer cylinder rotates to drive a fluid in the gap resulting in a shear stress on the inner cylinder surface which is measured as the torque applied to that cylinder by the fluid. Riblets of the desired size and shape are molded onto PVC adhesive film which is easily applied to (and removed from) the cylinder surfaces within the gap. Speeds of up to 4000 rpm are possible for the outer cylinder, allowing for a complete assessment of the riblet's performance in turbulent flow, and the gap size can be changed simply by using different diameter cylinders to increase the range of shear stresses investigated.

The discussion which follows describes the rotating cylinder drag balance and its accuracy in evaluating the drag characteristics of a selected riblet surface. Validation of the instrument was done by calibration to the exact solution for laminar flow and comparison of turbulent flow data to the historical results of G. I. Taylor (1936). Potential sources of error were considered, including frictional heating, end effects, and effects associated with the gap between the edges of the film applied to the cylinders. Riblets with a symmetric sawtooth profile were tested and, as will be shown, the instrument was able to predict drag reduction for this type of riblet in comparison to results reported in literature.

Received: 2 February 1999/Accepted: 1 October 1999

T. Hall, D. Joseph
Department of Aerospace Engineering and Mechanics
University of Minnesota, Minneapolis, MN

Correspondence to: D. Joseph

2 Description of instrument

A schematic of the rotating cylinder drag balance is shown in Fig. 1. It consists of two concentric cylinders with a fluid

annulus between them. The inner cylinder is made of nylon turned on a lathe to a specified diameter and the outer cylinder is made of 0.25 in. thick Plexiglas. The outer cylinder is attached to a drive belt and motor and rotates at a prescribed speed which is measured by a magnetic revolution counter (Hewlitt-Packard Counter Model 5316A). The inner cylinder is suspended freely by a shaft attached to a universal coupling, thus allowing the cylinder to move in any radial direction and self-center within the outer cylinder by hydrodynamic stability of the rotating fluid. Although the universal coupling is flexible, it is also designed to dampen vibrations of the inner cylinder resulting from instabilities in the fluid, which in turn minimizes fluctuations of the measured torque. The torque M is calculated from the load F applied to an Interface 10 lb. load cell with 0.0003 lb. resolution by a 3.5 in. moment arm attached to the coupling, as shown in Fig. 1. The shaft/moment arm system above the coupling is secured by two low-friction bearings spaced out by a steel frame (not shown in the diagram) to permit rotation about the axis of the cylinder but no radial movement above the coupling. A Constantine-Chromel thermocouple at the inner cylinder surface and attached to a Hewlitt-Packard 3478A Multimeter makes it possible to monitor the fluid temperature at that surface to account for changes in the fluid viscosity from frictional heating.

The instrument is designed so that both the inner and outer cylinder can be changed in order to study the effect of different cylinder radii and gap sizes. For the present investigation, the outer cylinder radius was held constant while four different inner cylinders were studied. These cylinder sets will be identified from now on as nos. 1–4 as specified by the dimensions given in Table 1. It should be noted that the cylinder radii listed include the thickness of the PVC film applied to them.

Two important parameters listed in Table 1 are the inner cylinder aspect ratio (L_i/R_i), which dictates the contribution of the end stress to the total stress on the cylinder, and the thickness ratio (b/R_o), which Taylor (1936) used as a measure of the flow's curvature. Under ideal conditions, $L_i/R_i \to \infty$ so that end effects are negligible and $b/R_o \to 0$ so that the flow is planar. Neither of these conditions are experimentally feasible for the rotating cylinder drag balance, but the cylinder lengths were made as large as possible within the frame of the instrument and the minimum gap size (3.00 mm) was selected to insure no potential contact between the cylinders when the flow is unstable. Nevertheless, these limitations do necessitate consideration of end effects and curvature as potential sources of inconsistency in the data and each is treated as such in the analysis and discussion of results which follows.

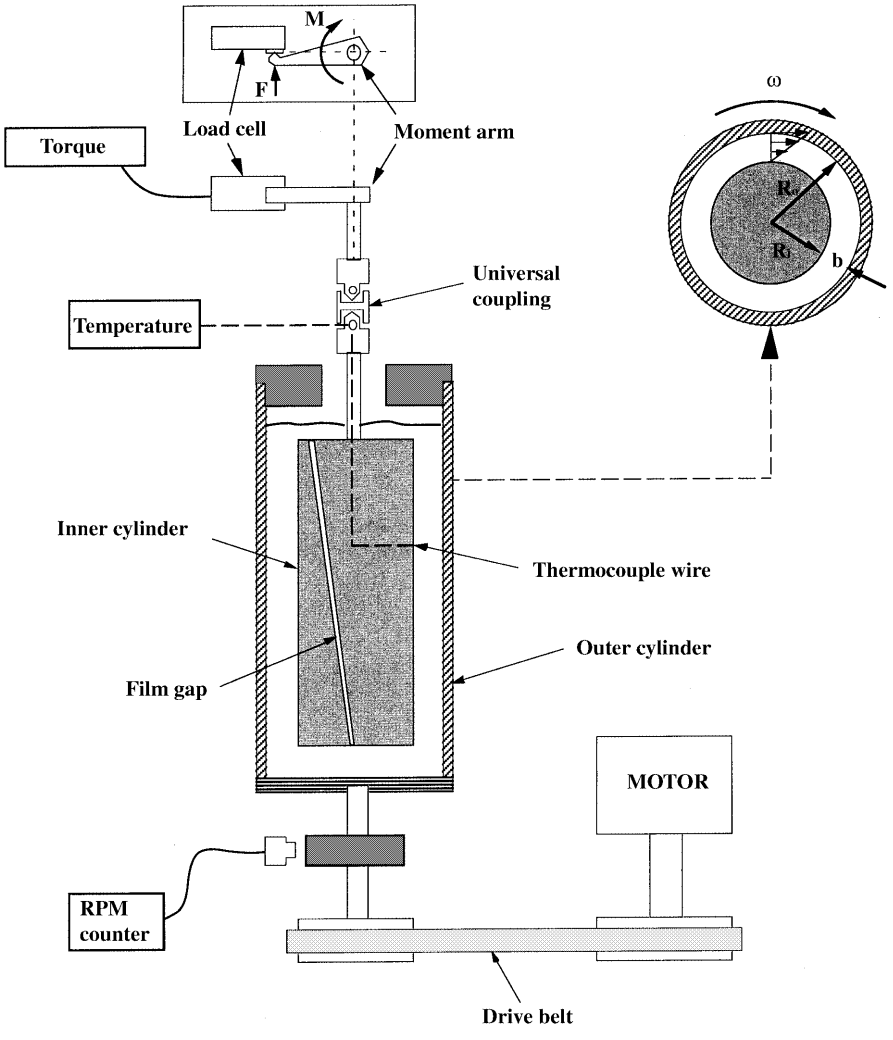

Fig. 1. Schematic of the rotating cylinder drag balance

Table 1. Cylinder sets and their relevant dimensions

Cylinder set	Inner cylinder radius R_i (mm)	Outer cylinder radius R_o (mm)	Inner cylinder length L_i (mm)	Gap size b (mm)	Aspect ratio L_i/R_i	Thickness ratio b/R_o
1	31.25	38.45	376.2	7.20	12.04	0.188
2	33.05	38.45	374.7	5.40	11.34	0.140
3	33.80	38.45	376.2	4.65	11.13	0.121
4	35.45	38.45	374.7	3.00	10.57	0.078

3 Potential sources of error

3.1 Frictional heating

When dealing analytically with problems involving Couette-type shear flows, it is convenient to treat the viscosity of the fluid between the boundaries as a constant, in which case the shear stress depends only on the velocity gradient in the gap. However, for many viscous liquids, it is necessary to take into account the dependence of the viscosity on the fluid temperature as well as the variation of the temperature throughout the gap due to frictional heating. Such a rise in temperature leads to a reduction in the fluid viscosity which in turn leads to less shear stress than anticipated in the fluid. This can be serious impediment to calibrating an instrument such as the one described here if the fluid used has a viscosity high enough that heating can occur even in laminar flow or is very sensitive to small temperature variations. In turbulent flow, the temperature rise can be quite dramatic (even in a low viscosity fluid like water) and cause the shear stress to continuously and rapidly decrease. Depending on the boundary conditions, this can also result in a complicated temperature profile within the gap, thus making it difficult to assign an average temperature to the fluid. Because of the severity of the consequences of frictional heating, it is worthy of a detailed analysis with an emphasis on obtaining accurate torque data when the temperature of the cylinders is not precisely known.

The shear stress τ at a given radial position r in laminar Couette flow between cylinders is given by:

$$\tau(r) = \frac{M}{2\pi r^2} = r\mu(T)\frac{\mathrm{d}}{\mathrm{d}r}\left(\frac{u(r)}{r}\right) \tag{1}$$

where M is the torque per unit length, $\mu(T)$ is the temperature dependent viscosity, and $u(r)$ is the azimuthal velocity. Integrating this gives:

$$\Omega_o - \Omega_i = \int_{R_i}^{R_o} \frac{M}{2\pi r^3 \mu(T(r;M))}\mathrm{d}r \tag{2}$$

where Ω_i and Ω_o are the angular speeds of the inner and outer cylinders, respectively. To obtain the dependence of M on Ω_i and Ω_o, it is necessary to determine the temperature $T(r)$ which satisfies the conduction equation with frictional heating, given by:

$$\frac{\mathrm{d}^2T}{\mathrm{d}r^2} + \frac{l}{r}\frac{\mathrm{d}T}{\mathrm{d}r} + \frac{M}{4\pi^2 k r^4 \mu(T)} = 0 \tag{3}$$

where k is the thermal conductivity and assumed constant. Note that the decrease of viscosity with temperature in liquids actually produces an increase in the dissipation. The nonlinear equation (3) must be solved together with boundary conditions appropriate to the particular fluid flow investigated. Under certain conditions when M is large, there are no solutions to Eq. (3), as verified by Joseph (1964). Under other conditions there may be two branches of solutions and only the branch with smaller temperatures is stable (Joseph (1965)).

Equation (3) shows that temperature $T(r)$ is maximum at any r for which $\mathrm{d}T/\mathrm{d}r = 0$. Moreover, the term $r\mathrm{d}T/\mathrm{d}r$ is a monotonically decreasing function of r. This implies that:

$$T_{\max} \geq T_{\mathrm{avg}} \equiv \frac{T(R_i) + T(R_o)}{2} \tag{4}$$

which subsequently means that there is a mean temperature $\bar{T} \neq T_{\mathrm{avg}}$ such Eq. (2) becomes:

$$\mu(\bar{T})(\Omega_o - \Omega_i) = \frac{M}{4\pi}\left(\frac{1}{R_i^2} - \frac{1}{R_o^2}\right) \tag{5}$$

Since $\bar{T} > T_{\mathrm{avg}}$ and $\mu(T_{\mathrm{avg}}) > \mu(\bar{T})$, then for fixed values of R_i, R_o, Ω_i and Ω_o, $M[T_{\mathrm{avg}}] > M[\bar{T}]$. Assuming that the maximum temperature $T_{\max}$ exists within the gap ($R_i < r < R_o$), then it can be further deduced that $M[T_{\max}] < M[\bar{T}]$.

For given values of Ω_i and Ω_o, the torque M is determined by the requirement that the solution $T(r;M)$ of Eq. (3) must also satisfy Eq. (2), which means M depends non-linearly on Ω_i and Ω_o. This can be done numerically by simultaneously solving these two equations in the following form:

$$\frac{1}{r}\frac{\mathrm{d}}{\mathrm{d}r}\left[r\mu\frac{\mathrm{d}u}{\mathrm{d}r}\right] - \frac{u}{r}\frac{\mathrm{d}\mu}{\mathrm{d}r} - \mu\frac{u}{r^2} = 0 \tag{6}$$

$$\frac{k}{r}\frac{\mathrm{d}}{\mathrm{d}r}\left[r\frac{\mathrm{d}T}{\mathrm{d}r}\right] + \mu\left[\frac{\mathrm{d}u}{\mathrm{d}r} - \frac{u}{r}\right]^2 = 0 \tag{7}$$

Computations were carried out using the code SIMPLER to solve Eqs. (6) and (7) for two sample fluids, with material parameters as specified in Table 2, between the

Table 2. Material parameters for the viscosity $\mu = \mu_o e^{-\gamma T}$ and the thermal conductivity k for fluids used in frictional heating analysis

Fluid	μ_o (kg/m s)	γ (°K^{-1})	K (kg m/s^3°K)
80 wt% glycerin in water	0.176	0.0540	0.326
Oil	1.098	0.0631	0.121

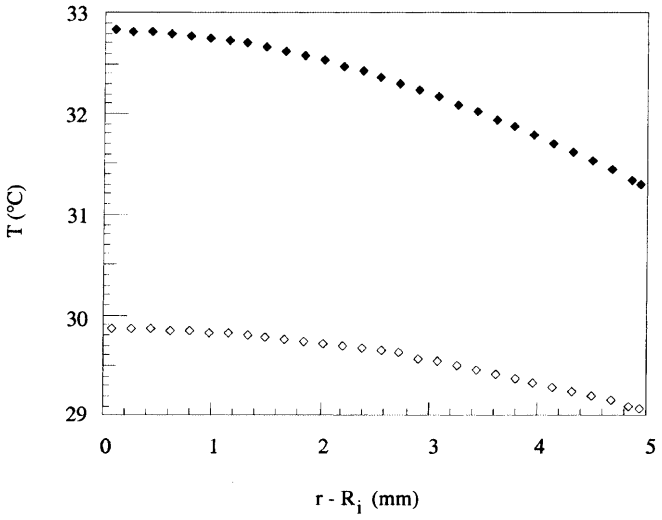

Fig. 2. Computed temperature distribution in the gap for 80 wt% glycerin in water at the following values of torque: ◆, $M = 0.1$ N-m; ◇, $M = 0.078$ N-m

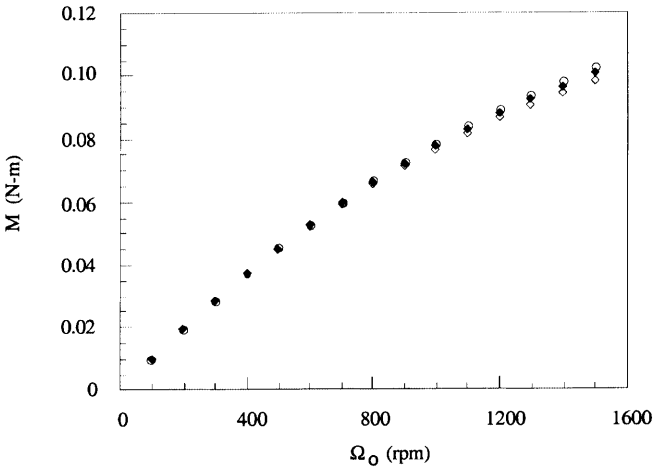

Fig. 3. Torque versus angular velocity for 80 wt% glycerin in water for the following cases: ◆, computed from Eqs. (6)–(9) taking frictional heating into account; ◇, computed from Eq. (5) with viscosity evaluated from $T(R_i)$; ○, computed from Eq. (5) with viscosity evaluated from T_{avg}

cylinders of set no. 2 (see Table 1). The boundary conditions for (6) are that $u = \Omega_i R_i$ and $\Omega_o R_o$ at the inner cylinder is stationary so that $\Omega_i = 0$. Equation (7) was solved for two different types of boundary conditions. In the first case it was assumed that there was no heat flux at the inner cylinder and the temperature T_o on the inside of the outer cylinder was connected to the temperature of the ambient air ($T_{amb} = 24.9\,^{\circ}C$ by heat conduction through the $t = 0.25$ in. thick Plexiglas using the heat resistance equation. Mathematically, these conditions are given by:

$$\frac{dT}{dr}\Big|_{R_i} = 0$$

$$-k\frac{dT}{dr}\Big|_{R_o} = k_p\frac{T_o - T_{wall}}{t} = h[T_{wall} - T_{amb}] \qquad (8,9)$$

where k_p is the thermal conductivity of the Plexiglas and T_{wall} is the temperature on the outer wall of the outer cylinder. The convective heat transfer coefficient h is given by the Nusselt number $Nu = hD/k_{air}$, where D is the outside diameter of the outer cylinder and k_{air} the thermal conductivity for air. The Nusselt number is evaluated from the following:

$$Nu_D = 0.18(0.5\,Pr\,Re_D^2)^{0.315} \qquad (10)$$

which is reported by Kreith (1968) as a correlation of experimental data for a rotating cylinder in air and is valid up to a Reynolds number of $Re_D = D^2\Omega_o/\nu = 4 \times 10^5$, where $\nu = \mu/\rho$ is the kinematic viscosity of air. The Prandtl number is given as usual by $Pr = \mu c_p/k$, where c_P is the heat capacity for air.

Figure 2 shows the temperature distribution computed for the 80 wt% glycerin solution for torque settings of 0.1 and 0.078 N-m based on the boundary conditions (8) and (9). Figure 3 compares the torque taking frictional heating into account with the torque of two constant viscosity fluids, one at the temperature T_i of the inner cylinder and the other at the average of the two surface temperatures

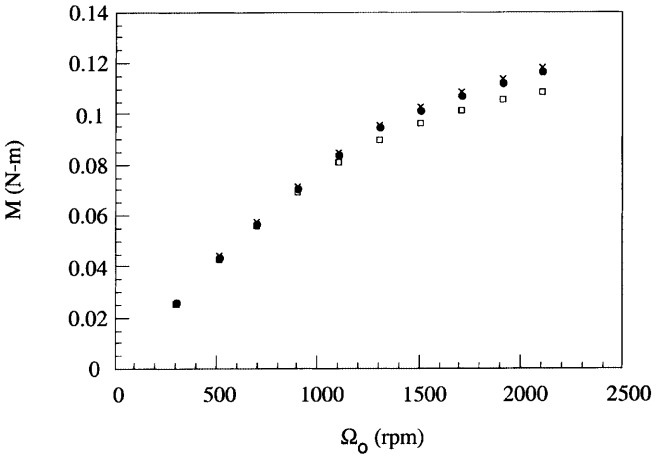

Fig. 4. Comparison of measured values of torque (×) for 80 wt% glycerin in water with values computed using the following conditions: □, viscosity evaluated from T_i ●, viscosity evaluated from T_{avg}

$T_{avg} = \frac{1}{2}[T_i + T_o]$. From the results it is clear that the average temperature works well but less and less well at higher speeds when the temperature increases significantly.

Experiments were performed with an 80 wt% glycerin in water solution in which the temperature was measured at the inside of the outer cylinder and the outside of the inner cylinder, using thermocouples embedded in each cylinder wall. (Note that the thermocouple in the rotating outer cylinder was eventually discarded due to difficulties in maintaining it.) The measured torque was represented fairly well by the average temperature T_{avg} with decreasing accuracy as the speed of rotation increased, as shown in Fig. 4. This experiment was flawed, however, because the inequalities $M[T_{avg}] > M[\bar{T}]$ and $M[T_{max}] < M[\bar{T}]$ deduced previously show that the measured torque should be between the torques computed using the average and maximum temperatures. This data is presented anyway as

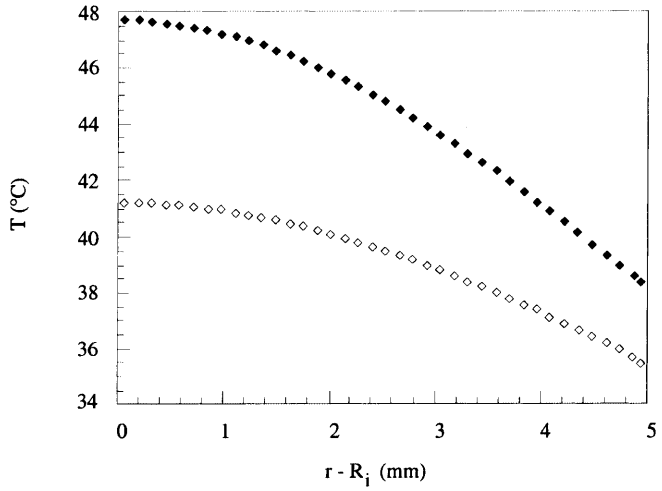

Fig. 5. Computed temperature distribution in the gap for oil at the following torque settings: ◆, $M = 0.21$ N-m; ◇, $M = 0.20$ N-m

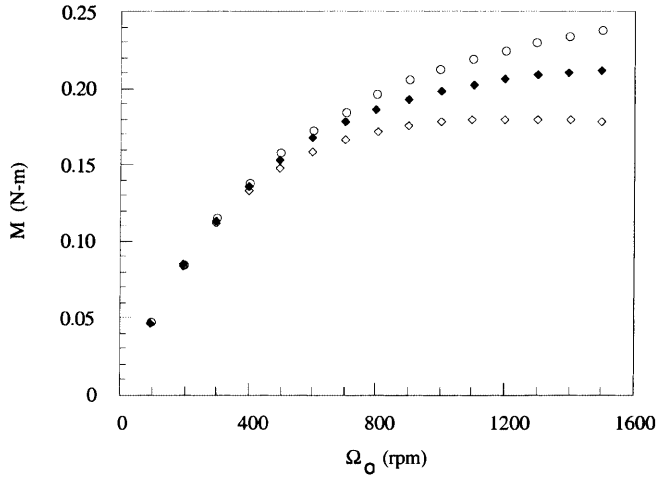

Fig. 6. Torque versus angular velocity for oil for the following cases: ◆, torque computed from Eqs. (6)–(9) taking frictional heating into account; ◇, torque computed from Eq. (5) with viscosity evaluated from T_i; ○, torque computed from Eq. (5) with viscosity evaluated from T_{avg}

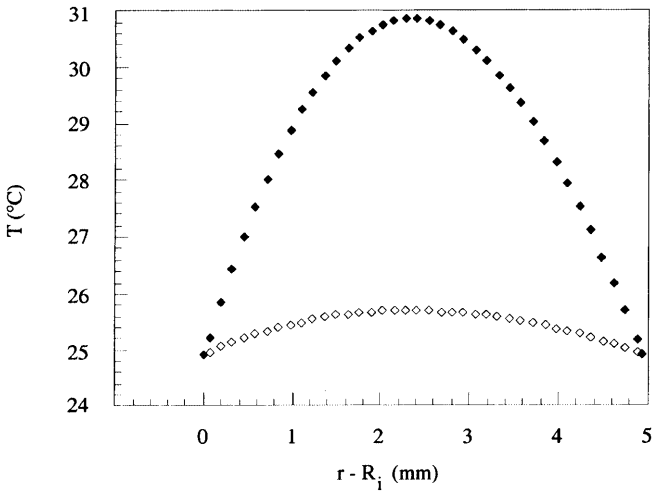

Fig. 7. Computed temperature distribution in the gap for oil at the following values of torque: ◆, $M = 0.567$ N-m; ◇, $M = 0.240$ N-m. The temperature at both cylinder surfaces is held constant at $T_i = T_o = T^* = 24.9\,^\circ$C

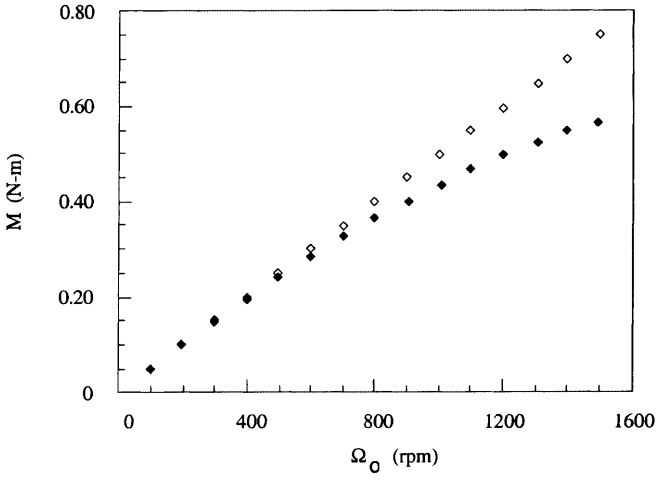

Fig. 8. Torque versus angular velocity for oil for the following cases: ◆, torque computed from Eqs. (6) and (7) with prescribed wall temperatures but taking frictional heating into account (i.e. changing viscosity); ◇, torque computed from Eq. (5) with constant viscosity evaluated from the prescribed wall temperature $T^* = 24.9\,^\circ$C

an example of how the theory should be used to critique an experiment. Possible causes for this discrepancy have not yet been explored.

Next, the oil mentioned in Table 2 was used to solve the system (6)–(9). The viscosity of this oil is far more sensitive to temperature than the glycerin-water solution, as is evident from the results plotted in Fig. 5. The temperature at the inner cylinder increases nearly 7 °C from an increase in torque of only 0.01 N-m. Figure 6 shows that it is impossible to predict the torque, even at moderate rotational speeds, if frictional heating is not accounted for when a fluid like this oil is used.

The next problem considered was whether viscous heating can be neglected or even suppressed by cooling the walls, in which case the second type of boundary condition for Eq. (7) is simply that the surface temperatures are prescribed and equal ($T_i = T_o = T^*$). Figure 7 shows computed values of the temperature distribution for the oil for torque settings of 0.567 and 0.240 N-m. Even with a controlled temperature at the cylinder surfaces, the temperature rise within the gap is quite dramatic when the torque is sufficiently large. The mean temperature in the gap ($\bar{T}$) will therefore increase with the torque and result in a fluid viscosity smaller than that estimated by the prescribed temperature T^*, which essentially means (as shown in Fig. 8) that the torque evaluated at T^* will be greater than that determined from an ever-changing mean temperature $\bar{T}$, and the disparity between them will therefore become greater as the angular speed increases.

Figure 9 shows the result of the calculation just presented but for the 80 wt% glycerin solution rather than the oil. The disparity in the data is still present but greatly diminished with significance only at rather high angular

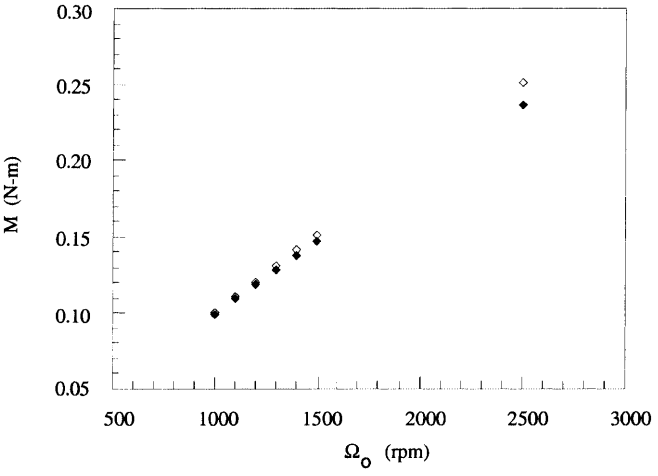

Fig. 9. Torque versus angular velocity for 80 wt% glycerin in water for the following cases; ◆, torque computed from Eqs. (6) and (7) with prescribed wall temperatures but taking frictional heating into account (i.e. changing viscosity); ◇, torque computed from Eq. (5) with constant viscosity evaluated from a prescribed wall temperature $T^* = 24.9\,^{\circ}\mathrm{C}$

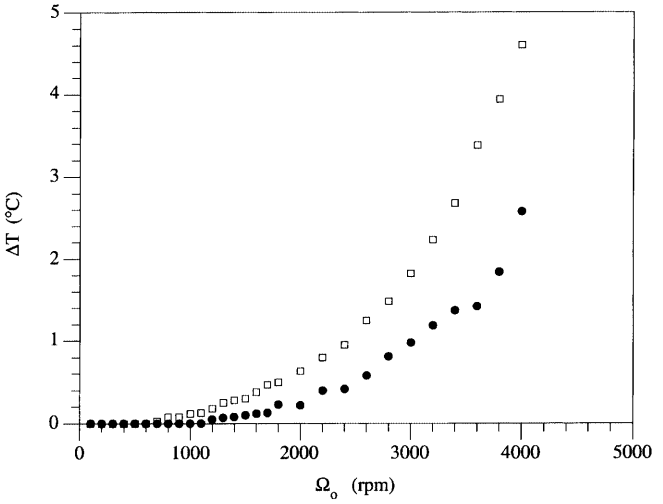

Fig. 10. Rise in temperature at the inner cylinder surface for cylinder set no. 4 and for the cases of: □ = successive measurements: ● = "one at a time" measurements. For the former case, the approximate time between measurements was 15 s. For the latter case, the water annulus was allowed to cool for 30 min between measurements, and the time to achieve the desired speed and a steady state torque measurement was 30–60 s (increasing with higher speeds)

speeds. In general, the glycerin solution has a less sensitive viscosity as well as a higher thermal conductivity than the oil. A higher k implies that heat is transferred more rapidly from the fluid to the boundaries resulting in a less prominent temperature profile in the gap and a smaller mean temperature, which ultimately means less disparity between the torque estimated from the wall temperature and that from when frictional heating is accounted for.

The conclusion from this analysis is that the ideal fluid for the rotating cylinder drag balance, at least from the perspective of accurately calibrating the instrument for laminar flow, is one with high thermal conductivity and a viscosity with low sensitivity to temperature variations, and it is for this reason that all experiments performed with the instrument were limited to water ($k = 0.609$ kgm/s$^{3^{\circ}}$K) and moderate concentrations of glycerin (20 wt% and 44 wt%). For these fluids, laminar flow was observed for outer cylinder angular speeds of up to 350 rpm for water and 850 rpm for 44 wt% glycerin. No significant temperature rise was measured at the inner cylinder surface at these relatively low speeds, as verified for water in Fig. 10, and therefore made it possible to avoid frictional heating effects and allow for precise calibration of the instrument.

While the above analysis focused on how frictional heating effects fluids in laminar flow, it is a far more complicated issue when considering the same in turbulent flow, for which the rate of heat generation increases dramatically at high angular speeds, even for low viscosity fluids like water. Since the primary function of the instrument as it is described here is to study surfaces in turbulent flow, regulating frictional heating in this flow regime is far more critical to its proper operation. Unfortunately, methods by which to do this are non-existent without severely changing the complexity of the instrument. The only feasible location for a thermocouple is at the inner cylinder surface and the temperature at the outer cylinder can be roughly estimated at best, making it is impossible to predict the variation in viscosity throughout the gap and assign an accurate mean viscosity to the fluid. The temperature rise depends both on the speed of rotation and the length of time it rotates at the speed, and so if torque measurements over a range of outer cylinder speeds (0–4000 rpm in intervals of 200 rpm, for example) are done in succession, frictional heating will increasingly become a problem as the test progresses. The only way to combat this issue is to simply take a "one measurement at a time" approach, that is, to take a measurement at a given speed and then shut down the device and allow the fluid to cool before making the next measurement. This is not an end-all solution to the problem since it does take some time (up to 60 s) to accelerate the outer cylinder to speeds of 3000–4000 rpm and during that time the fluid temperature does increase. However, this increase is moderately less than that experienced during successive measurements, as is shown in Fig. 10, and so the error in specifying the fluid viscosity by the inner cylinder surface temperature is at least minimized.

3.2
End effects of inner cylinder

Because the inner cylinder is suspended freely within the outer cylinder, there is a fluid gap between the ends of each and it is reasonable to assume that some of the stress on the inner cylinder might be contributed by the shear flow in this region. The top of the outer cylinder is open such that the fluid in this region is essentially in a free shear flow and therefore should have little effect on the top of the inner cylinder or the thin shaft connecting it to the coupling. The bottom of the outer cylinder, however, does rotate to create a shear flow between itself and the inner cylinder bottom. For laminar flow, the torque exerted on a disk of radius R_i by another disk rotating a distance h above it is given by:

$$M_{\text{disk}} = \int \tau r \, dA = \int_0^{2\pi} \int_0^R \tau r^2 \, dr \, d\theta \tag{11}$$

where τ is the shear stress and equal to:

$$\tau = \mu \frac{du}{dz} = \mu \frac{r\Omega_o}{h} \tag{12}$$

where Ω_o is the angular speed in radians per second. Substituting (12) into (11) and integrating gives:

$$M_{\text{disk}} = \frac{\pi}{2} \frac{\mu \Omega_o R_i^4}{h} \tag{13}$$

The torque on the rest of the cylinder in laminar flow is given by Eq. (5). Assuming constant viscosity and noting that the torque in that equation is per unit length of cylinder, this gives:

$$M_{\text{cyl}} = ML_i = \frac{4\pi\mu\Omega_o L_i}{\left(\frac{1}{R_i^2} - \frac{1}{R_o^2}\right)} \tag{14}$$

where L_i is the length of the inner cylinder. From (13) and (14), the contribution of torque from the bottom of the inner cylinder is then:

$$\frac{M_{\text{disk}}}{M_{\text{cyl}}} = \frac{1}{8hL_i} \left(\frac{R_i^2}{R_o^2}\right)(R_o^2 - R_i^2) \tag{15}$$

Based on this relation, the end effects of the inner cylinder can be minimized (assuming the radii of the cylinders are fixed) by maximizing either the length (L_i) of the cylinder or the size of the gap (h) between the ends. The former case obviously makes sense since under ideal conditions it is assumed the cylinder is infinitely long. G. I. Taylor admitted to neglecting end effects in his research but assumed the error negligible since his inner cylinder aspect ratio was very large ($L_i/R_i \approx 20.8$). In the present case, the cylinder length is restricted by the size of the instrument frame but nevertheless was chosen to be as large as possible.

There was also limited flexibility in choosing the bottom gap height because of restrictions on the length of the outer cylinder. It was necessary to experimentally determine the allowable size of this gap for end effects to be minimized. Once again, the complexity of turbulent flow plays a role here, particularly since it is a three-dimensional flow for which Eqs. (11)–(15) are not applicable and temperature variations in the fluid in this region may not comply to those experienced in the radial gap. Figure 11 shows the torque versus angular speed for different bottom gap sizes, from which $h \approx 1.5$ cm is established as the minimum value for which end effects are nominal.

3.3 Film Gap Effects

The surface characteristics of the cylinders are controlled through the application of Scotchcal® High Performance PVC film. It is used in both riblet form and smooth form, the latter being the control surface to which riblet performance is evaluated. The film must be applied to the cylinders by a manual process requiring the adhesive side of the film to be wetted with soapy water and then wrapped

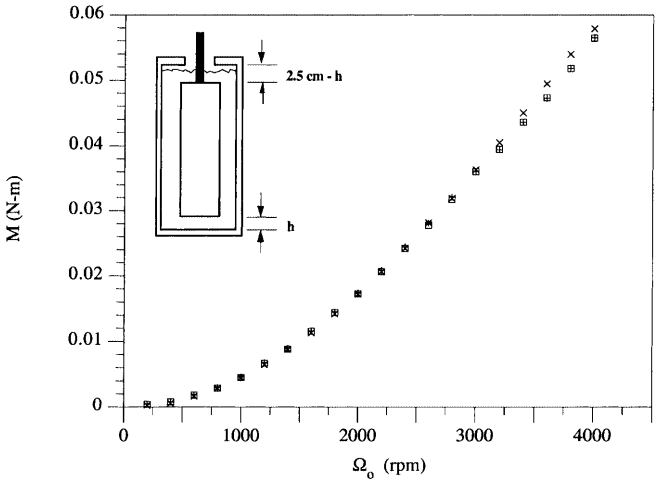

Fig. 11. Effect of the gap (h) between the end of the inner and outer cylinders on the measured torque M for cylinder set no. 2. ×, $h = 0.5$ cm; □, $h = 1.5$ cm; +, $h = 2.0$ cm

on carefully to avoid air pockets. This is difficult process and it is impossible to insure that the edges of the film meet perfectly along the entire length of the cylinder. Thus, it is necessary to trim the film to be slightly smaller than the circumference of the cylinder, resulting in a gap between the film edges of approximately 1.0 mm in width. Despite the fact that the smooth film is only 64 μm thick, this gap still represents a discontinuity in the cylinder surface which may act as a form of roughness and increase the stress on the surface.

If the film is applied such that this gap is parallel to the inner cylinder axis (i.e. perpendicular to the direction of flow), the entire length of flow would experience adverse effects from this surface discontinuity at the same azimuthal location. This could cause the flow to lose its axisymmetry and ultimately distort the torque measured on the inner cylinder. It was proposed that any such error could be minimized by displacing the film gap so that it wrapped around at least a portion of the cylinder, as displayed in the schematic of the instrument in Fig. 1. This presumption was tested by measuring the torque on a given cylinder when the film gap was aligned vertically and then progressively at an angle with respect to the cylinder axis. No film was applied to the outer cylinder for these tests in order to isolate the error associated with a single film gap.

The alignment of the film gap is described by the parameter δ, representing the circumferential distance the film gap wraps around the cylinder, as shown on the diagram in Fig. 12. This figure also shows the resulting data, which indicates that there is an increase in torque corresponding to the alignment of the film gap and that the error can be reduced by angling this gap. For the case of a vertical film gap ($\delta = 0$), there was an apparent instability in the flow, as seen by oscillations of the inner cylinder and minor fluctuations of the torque measurements, which became gradually more noticeable as the outer cylinder speed was increased. The data converges when $\delta \geq 4$ cm, which for cylinder set no. 4 is equivalent to 18% of the inner cylinder circumference. This convergence of data

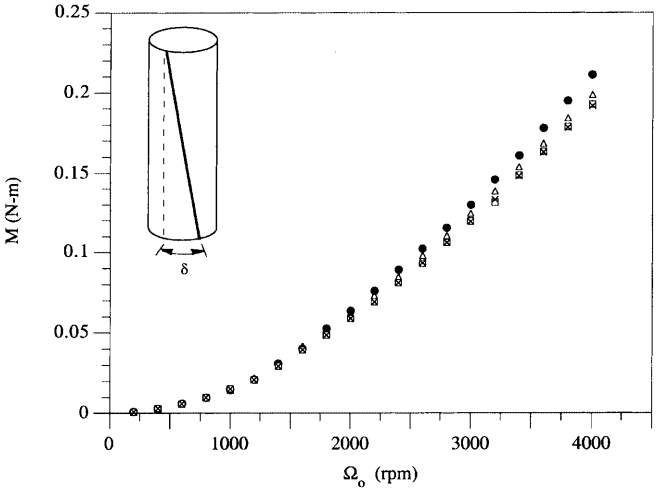

Fig. 12. Effect of the film gap's alignment on the measured torque M for cylinder set no. 4. The parameter δ is the arc length of the gap from the ends of the cylinder. ●, $\delta = 0$ (vertical gap); Δ, δ = 2 cm; □, δ = 4 cm; ×, $\delta = 8$ cm

was verified with cylinder set no. 2 for which the oscillations of the inner cylinder were not nearly as noticeable and showed no effect on the torque, suggesting that a larger radial gap minimizes the influence of this film gap on the surface stress.

4
Instrument validation

4.1
Relevant parameters

The parameters of choice for analyzing data collected from the rotating cylinder drag balance when the cylinders are covered with smooth film are Reynolds number and skin friction coefficient, defined respectively by:

$$\mathrm{Re} = \frac{\rho U_o b}{\mu(T_i)} \tag{16}$$

$$c_f = \frac{\tau}{\frac{1}{2}\rho U_o^2} \tag{17}$$

where ρ is the fluid density, U_o the velocity of the outer cylinder, b the radial gap size, $\mu(T_i)$ the viscosity as a function of the inner cylinder surface temperature, and τ the shear stress on the inner cylinder. In terms of the measurable parameters of outer cylinder angular speed Ω_o (in units of rpm) and torque M, the velocity and shear stress are given by:

$$U_o = \frac{\pi}{30}\Omega_o R_o \tag{18}$$

$$\tau = \frac{M}{2\pi R_i^2 L_i} \tag{19}$$

where R_i and R_o are the inner and outer cylinder radii and L_i is the inner cylinder length. Substituting (18) and (19) into (16) and (17) gives the desired relations:

$$\mathrm{Re} = \frac{\pi\rho b R_o}{30\mu(T_i)}\Omega_o \tag{20}$$

$$c_f = \frac{\pi}{R_i^2 R_o^2 L_i}\left(\frac{M}{\Omega_o^2}\right) \tag{21}$$

4.2
Laminar flow

The exact solution for laminar flow is given by Eq. (14) for the torque as a function of the outer cylinder angular speed. In terms of Reynolds number and skin friction coefficient, as given by (20) and (21), the laminar flow solution becomes:

$$c_f = \left(\frac{2R_o}{R_i + R_o}\right)\frac{2}{\mathrm{Re}} \tag{22}$$

where the term in parentheses is the result of curvature in the flow.

4.3
Turbulent flow

Although M.M. Couette in 1890 was the first to study the cylindrical shear flow for which his namesake was given, it is the work of G. I. Taylor which is of most interest to the present investigation, primarily because of the comparable scale of his experimental apparatus to the one used here. In the sixty years since Taylor's work, there has been interest in cylindrical Couette flow when the outer cylinder rotates while the inner remains stationary, with the focus instead being on the opposite case for which patterned instabilities (Taylor vortices) are present. Taylor's results must therefore serve as the benchmark by which to assess the validity of the present data, particularly in the turbulent flow regime.

Taylor made torque measurements on cylinder sets with radial gaps ranging from 1.10 to 8.55 mm using water, glycerin solutions, pentane, and aviation spirits as his test fluids. His outer cylinder had an inside radius of 40.6 mm, which is 5.5% larger than the outer cylinder used here. Although these radii are reasonably similar, it does not guarantee a comparison of his data to the present data for the same gap size, primarily because the larger radii will correspond to approximately 5.5% less curvature in the flow. Taylor observed that increasing the curvature, which he described by the thickness ratio b/R_o, caused the data when plotted in dimensionless for (Re vs. c_f) to shift down the line representing the laminar flow solution (22). This is justified by the fact that, for a constant outer cylinder radius, and increase in curvature means an increase in the gap size, resulting in less torque on the inner cylinder and, in turn, smaller values of c_f. Taylor treated the thickness ratio as the distinguishing parameter for data from different gap sizes, and it serves a similar purpose here, instead of the gap size, when comparing results to those of Taylor because of the slight difference in cylinder dimensions.

4.4
Discussion of results

Experimental results are provided in Figs. 13–16 for the four cylinder sets with smooth film on both cylinders. In each case, data is reported for two separate tests of water

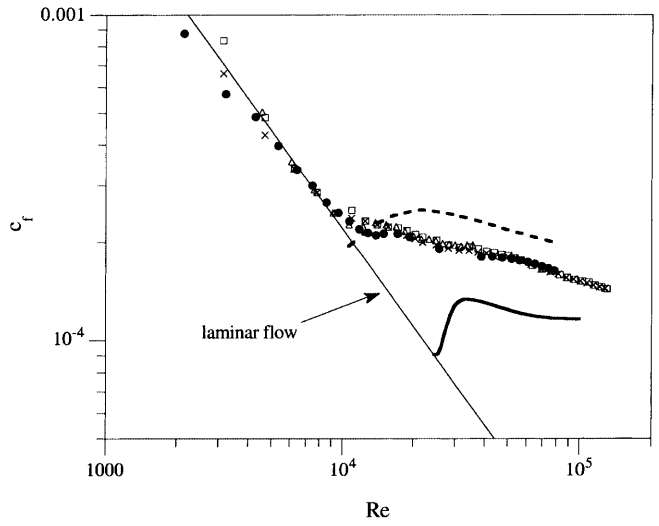

Fig. 13. Skin friction data for cylinder set no. 1 ($b/R_o = 0.188, b = 7.20$ mm) and the following liquids: □ = water (test no. 1); × = water (test no. 2); ● = 20 wt% glycerin; Δ = 44 wt% glycerin. Taylor's data: - - - - $b/R_o = 0.148$;—- $b/R_o = 0.211$

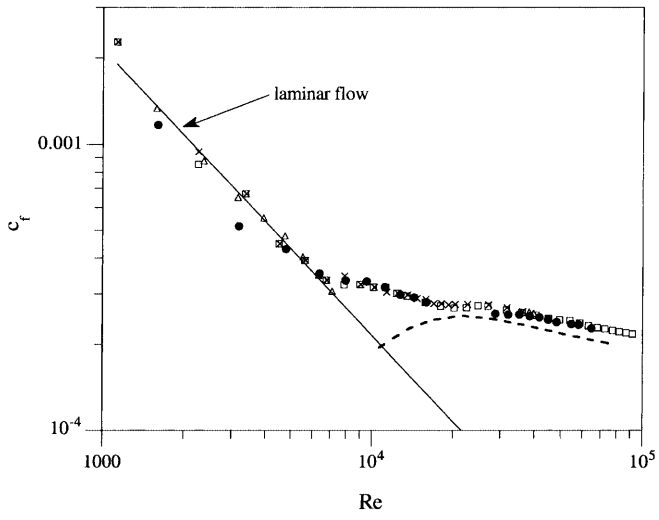

Fig. 14. Skin friction data for cylinder set no. 2 ($b/R_o = 0.140, b = 5.40$ mm) and the following liquids: □ = water (test no. 1); × = water (test no. 2); ● = 20 wt% glycerin; Δ = 44 wt% glycerin. Taylor's data: - - - - $b/R_o = 0.148$

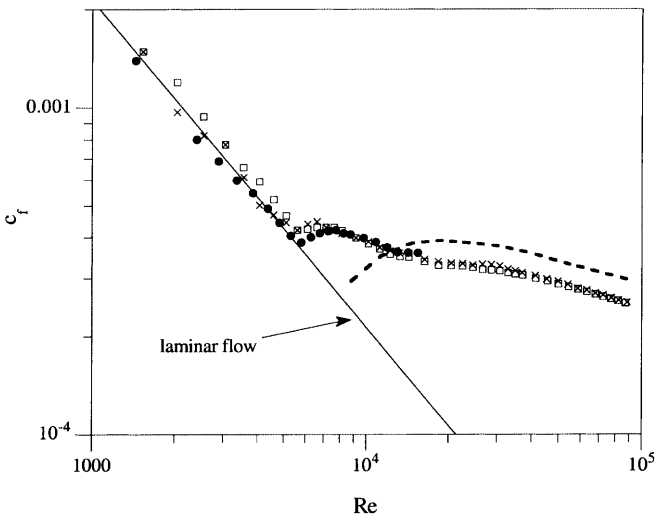

Fig. 15. Skin friction data for cylinder set no. 3 ($b/R_o = 0.121, b = 4.65$ mm) and the following liquids: □ = water (test no. 1); × = water (test no. 2); ● = 44 wt% glycerin. Taylor's data: - - - - $b/R_o = 0.115$

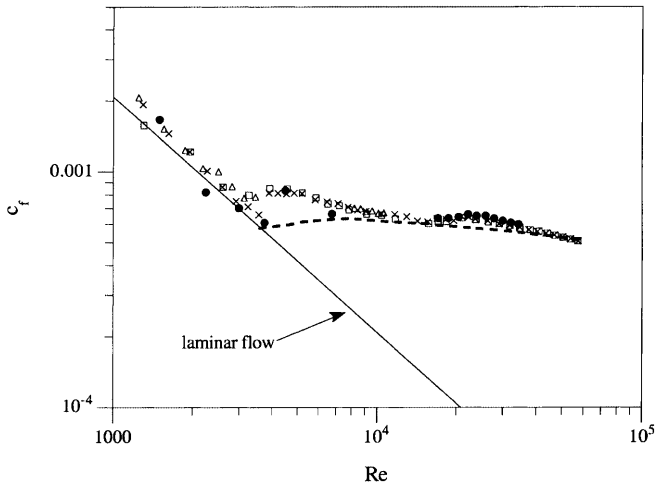

Fig. 16. Skin friction data for cylinder set no. 4 ($b/R_o = 0.078, b = 3.00$ mm) and the following liquids: □ = water (test no. 1); × = water (test no. 2); ● = 20 wt% glycerin; Δ = 44 wt% glycerin. Taylor's data: - - - - $b/R_o = 0.078$

to show the repeatability of results and for aqueous glycerin solutions (20 wt% and/or 44 wt%) to show the consistency of the results for different test fluids. Also shown in each plot is the exact solution for laminar flow and Taylor's results for thickness ratios closest to that of the respective cylinder set. It should be noted that Taylor's curves are not the author's interpretation of his data but rather replications of the actual curve fits reported by Taylor (1936).

It can be seen from the data that there is a clear transition to turbulence as indicated by the sudden deviation from the laminar flow solution and subsequent rise in value of the skin friction coefficient. This transition consistently occurs at smaller Reynolds numbers than those reported by Taylor, suggesting that something in the design of the present instrument is triggering premature instabilities is the flow. Two potential sources are the film gap and the sharp edges at the ends of the inner cylinder, with the latter being the more likely candidate. A crude flow visualization was performed by adding neutrally buoyant glass micro-spheres to the test fluid, from which it was observed that instability in the flow at the time of transition first appeared at the cylinder edges and with a far greater intensity at the bottom edge. Taylor's cylinders were considered smooth as is and his inner cylinder spanned the length of the outer cylinder such that he could avoid potential triggers of instability and allow the flow to remain laminar for as long as possible.

After the transition region, the flow gradually becomes fully turbulent and the skin friction coefficient again

steadily decreases with increasing Reynolds number but at a lesser slope than in laminar flow, thus giving the typical Bode plot response for shear flows. For all four cylinder sets, however, there is an uncharacteristic "dip" in the data occurring at around Re = 10000–30000, and for decreasing gap size this dip becomes far more conspicuous and occurs further away from the transition region. The reason for this anomaly is not clearly known, though it is interpreted as a temporary reduction in the drag on the inner cylinder potentially by a decrease in the intensity of the turbulence. During testing it was observed that the inner cylinder experiences high frequency oscillations during the range of Re for which this dip occurred. When water was the test fluid the oscillations were minor in amplitude and did not interfere with measuring the torque, but for the more viscous 44 wt% glycerin the severity of the oscillations were such that a consistent torque measurement was impossible for most of the angular speeds within this range. It was also observed for the case of water that the oscillations became more prominent as the gap size decreased, which correlates with the fact that the dip is most significant for cylinder set no. 4 (having the smallest gap) and implies a relation between the oscillations and the temporary reduction in drag. It is possible that the flow is not fully turbulent in this range causing a stress imbalance on the inner cylinder. This imbalance is compensated for by the cylinder's freedom to move in the radial direction, thus leading to the oscilations. Ultimately, this may serve as a dynamic method of drag reduction which disappears once the flow becomes fully turbulent and the stress imbalance is eliminated. Flow visualization using the micro-spheres could not support this claim because of the high speed of the flow, and clearly more research is necessary to understand this phenomenon. Regardless, the data for all cylinders indicates that the dip region is at least repeatable when is the test fluid and subsequently had no major influence on the results for riblet film.

Overall, the turbulent flow data is consistent with Taylor's results, specifically in how decreasing curvature in the flow ($b/R_o \to 0$) increases the magnitude of the drag coefficient and the slope at which c_f changes with increasing Reynolds number. In the case of cylinder set no. 4, the only one for which the thickness ratios are equivalent, there is very good agreement with Taylor's results at high Reynolds number. The excellent repeatability of the data for water, particularly in the turbulent flow range, makes it the ideal test fluid for the instrument.

5 Drag reduction using riblets

5.1 Relevant parameters

Drag reduction due to riblets is traditionally described by the riblet spacing Reynolds number and the stress reduction ratio, defined respectively by:

$$S^+ = \frac{su^*}{v} \tag{23}$$

$$\frac{\Delta\tau}{\tau_o} = \frac{\tau_{rib} - \tau_o}{\tau_o} \tag{24}$$

where s is the spacing between riblet tips (see Fig. 17 below), v is the kinematic viscosity, τ_{rib} and τ_o are the shear stress on inner cylinder for riblets and smooth film, respectively, and u^* is the friction velocity, given by:

$$u^* = \sqrt{\frac{\tau_o}{\rho}} \tag{25}$$

5.2 Historical results

The riblets tested in the drag balance were of the type with triangular cross-section, also known as sawtooth or V-groove riblets, as shown in Fig. 17. They have symmetric grooves such that both the height h and spacing s are equal to 114 μm. This style of riblets has been widely studied in the past by many researchers in both wind tunnels and fluid channels, and a survey of their experimental data has been compiled by Walsh (1990). The general consensus of their results is that riblets of this type produce drag reduction in the manner shown in Fig. 18. Specifically, there is a range of riblet spacing Reynolds numbers for which drag reduction is present, roughly $3 < S^+ < 22$, and outside of this range there is a drag cost which becomes more and more severe, especially for large values of S^+. The maximum amount of drag reduction occurs in the range $10 < S^+ < 15$ with a value of approximately 5.0%. (Bechert et al. (1997) reports a precise value of 5.1% with these riblets.) The goal of the present investigation, therefore, was to show that the rotating cylinder drag balance could

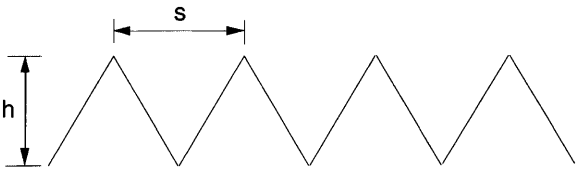

Fig. 17. Sawtooth riblets with height h and tip spacing s

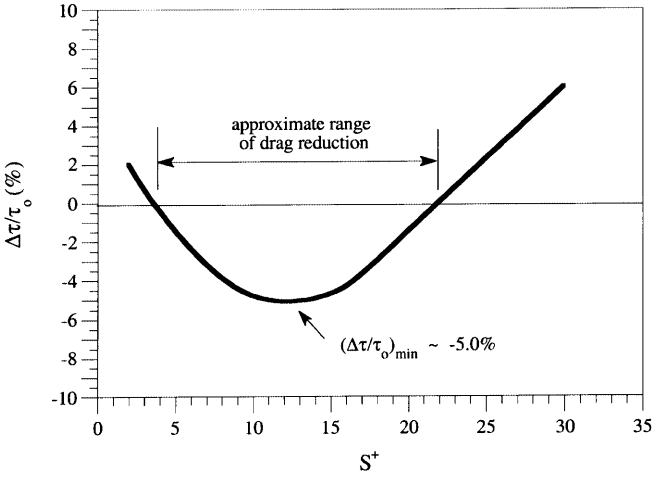

Fig. 18. Typical drag reduction from sawtooth riblets ($h = s = 114\,\mu m$)

predict similar drag reduction with reasonable accuracy and specifically provide data resembling the curve in Fig. 18.

5.3
Experimental considerations with riblets

When measuring the drag on surfaces like riblets, an important issue is how to simulate the riblet surface within the boundaries of the selected experimental apparatus. This depends both on the arrangement of the facility and the method used for measuring the drag.

For instance, in a wind tunnel the test surface is typically replicated on a flat plate attached to a strain gauge, and in a recirculating pipeline the riblets are applied to the entire circumference of the pipe and the pressure drop over a specified length is measured. For the rotating cylinder drag balance, however, the application of the riblet film is not quite as straightforward since there are two surfaces to consider, the one which drives the flow (outer cylinder) and the one for which the actual shear stress is measured (inner cylinder). Because the influence of riblets is localized, that is, they reduce the span-wise turbulence intensity near the surface and increase the thickness of the viscous sublayer, it would seem to suffice to apply riblets only to the only to the cylinder for which the drag is measured. However, riblets on the outer cylinder should have a similar effect on the fluid near that surface, and since the shear stress applied to the inner cylinder is the product of momentum transfer through the fluid gap from the moving outer cylinder, it is intuitively implied that riblets on either surface should have some influence on the measured drag.

Under "ideal" conditions (i.e. planar flow), the result of having riblets on both surfaces would be to double the effect on the drag in comparison to having riblets on only one surface. However, Eq. (1) indicates that in a curved flow the shear stress varies with the inverse square of the radius, which means the shear stress at the outer surface will always be less than at the inner surface. This leads to the hypothesis that curvature should reduce the drag reduction attributed to riblets at the outer surface with less and less benefit as the curvature is increased. To address this issue, it was necessary to test all possible combinations of riblet and smooth film (i.e. riblets only on inner cylinder, only on outer cylinder and on both cylinders) to determine which best reproduces results from literature.

5.4
Discussion of results

Figure 19 shows drag reduction data for all cylinder sets for riblet film on the inner cylinder and smooth film on the outer cylinder and with water as the test fluid. In general, drag reduction is predicted by all four cylinder sets, but the results which best depict those reported by Walsh (1990) are for cylinder set no. 4, as is evident by the near perfect resemblance of the least squares curve fit for this data and the curve shown in Fig. 18. The range of drag reduction is approximately $5 < S^+ < 20$ with a maximum reduction of about 5–6% detected in the range $9 < S^+ < 13$. While the results for cylinder set no. 2 and no. 3 are fairly consistent with those for no. 4, there is a

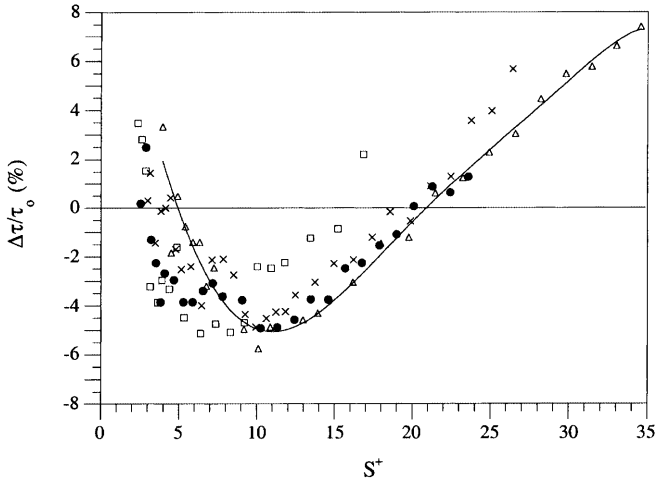

Fig. 19. Percent change in shear stress as a function of the riblet spacing Reynolds number for the case of riblet film on the inner cylinder and smooth film on the outer cylinder. □ = cylinder set no. 1; ● = cylinder set no. 2; × = cylinder set no. 3; Δ = cylinder set no. 4. Smooth curve is a least squares fit of the data for cylinder set no. 4

clear trend in the data which first appears for these cylinder sets and becomes most evident with the data for cylinder set no. 1. For increasing curvature in the flow, the characteristic drag reduction curve appears to shift down the S^+ scale, that is, maximum drag reduction is predicted at a smaller S^+ and the upper limit for any drag reduction at all also decreases. The most severe case is for cylinder set no. 1, which still gives a maximum reduction of around 5% but in the range $6 < S^+ < 9$ and shows a rise in drag as early as $S^+ = 15$. The trends in this data support the fact that minimizing the curvature provides the most accurate results, and certainly the ideal case would be to test the riblet film in planar Couette flow. However, achieving small curvature means minimizing the gap between the cylinders, which consequently means increasing the risk of contact between the cylinders when the flow is unstable. Therefore, it is concluded that the most accurate possible drag reduction results achievable by this instrument are those obtained from cylinder set no. 4.

It is interesting to note from Fig. 19 that for $S^+ < 5$ the drag is actually enhanced. This is not a unique result since Walsh's data shows a similar rise in drag for small S^+, but nevertheless its occurrence here must be addressed. The implication is that at the onset of turbulence (i.e. just after transition) the riblets promote drag, despite the fact that in laminar flow (i.e. just prior to transition) there is no such difference between riblets and smooth data. One potential explanation for this is simply experimental error, possibly by the poor resolution of the torque-measuring load cell (0.0003 lb) at the low levels of stress encountered in this flow range. However, the consistent occurrence of the drag rise after, but not before, transition leads to speculation that something in the flow behavior could be involved. It is possible that the height of the viscous sublayer just after transition may be insufficient to deter the influence of the riblet peaks on the turbulent shear stress applied to the surface. Once the "exposed" surface area is minimized (upon maturity of the sublayer) the

reduction in drag is initiated. This is presented here merely as an empirical interpretation of the phenomenon and there is no historical evidence to support these statements (Walsh does not address the cause of the drag rise). For now the importance of the data in Fig. 19 and subsequent figures is the S^+ range for which drag reduction is measured.

Figures 20 and 21 show results of similar tests for the respective cases of riblet film only on the outer cylinder and on both cylinders, from which it is evident that neither case provides useful information regarding the performance of the riblets. For riblets only on the outer cylinder, drag reduction is predicted for each cylinder set but is present over a very limited range of S^+ and maximum reduction is only 3–4%. There is also a very inconsistent distribution in the data, especially for $S^+ < 10$. The fact that any drag reduction is predicted for this case does

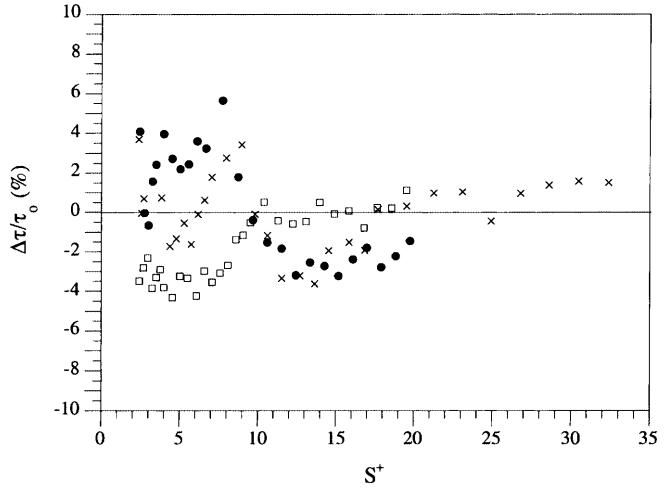

Fig. 20. Percent change in shear stress as a function of the riblet spacing Reynolds number for the case of smooth film on the inner cylinder and riblet film on the outer cylinder. □ = cylinder set no. 1; ● = cylinder set no. 2; × = cylinder set no. 4

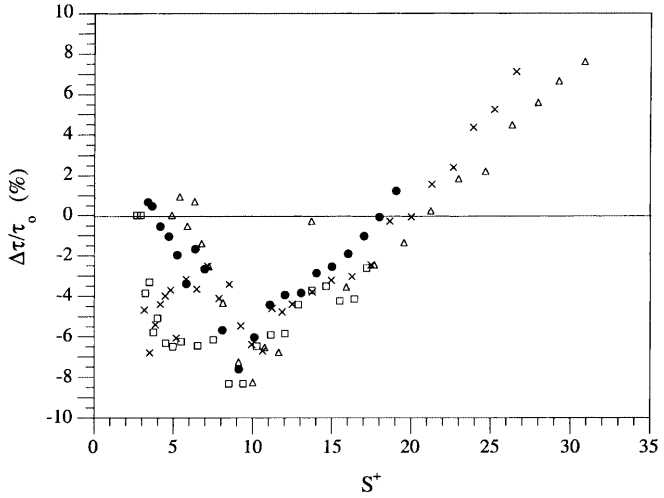

Fig. 21. Percent change in shear stress as a function of the riblet spacing Reynolds number for the case of riblet film on both cylinders. □ = cylinder set no. 1; ● = cylinder set no. 2; × = cylinder set no. 3; Δ = cylinder set no. 4

suggest that, as speculated before, the benefit of riblets is more far-reaching than the near-wall region where the riblets are applied. Nevertheless, the results for this case do not nearly resemble the consistency seen for the case of riblets on the inner cylinder and basically have no value in predicting the riblet performance.

Similarly for the case of riblet film on both cylinders, it appears that the presence of riblets at the outer surface has some influence on the stress measured at the inner surface. To some extent it enhances the performance of the inner cylinder riblets, increasing the maximum drag reduction to approximately 6–8% in the range $8 < S^+ < 12$. It is difficult to interpret these results, since the data shows no clear trend to support the previous statement that increasing curvature will reduce the stress at the outer cylinder surface and therefore should reduce the benefit of riblets on that surface. Also, from a practical standpoint these results cannot be applied to other flow situations with different boundaries (i.e. external flows) and therefore are of no value in predicting riblet performance, except perhaps in situations involving rotating shear flows. For now, the positive results for the case of riblets only on the inner cylinder are sufficient for showing the instrument's ability to predict small drag reductions.

6
Concluding remarks

The preceding discussion has shown by validation and demonstration with riblets that the rotating cylinder drag balance can serve its function as a surface drag measuring device with reasonable accuracy. Skin friction data agrees well with the historical results of Taylor and is repeatable, particularly at high Reynolds number, for the case of water as the test fluid. Water has proven to be the most suitable choice for testing, not only for the previous point, but also because its low viscosity and high thermal conductivity make it most resistant to substantial temperature rises due to viscous heating in turbulent flow. Application of the desired test surface to only the inner cylinder and selecting cylinders with the smallest curvature possible allow for the most reliable assessment of that surface's drag properties.

There are still questions regarding the behavior of the flow between the cylinders, such as why there is a mysterious dip in the skin friction data after transition and how it can be eliminated, but these are left for future consideration. Despite these issues, the instrument still predicts the drag reducing properties of riblets with an accuracy on the same order as results reported in literature. When accounting for the overall simplicity of its design, the minimal amount of material necessary to test a given surface, and the fact that it is small, self-contained and relatively inexpensive to operate, the rotating cylinder drag balance has many advantages over, and may even be preferable to, more complex experimental facilities including wind tunnels.

Although the rotating cylinder drag balance has been presented here as a tool for predicting drag reduction due to riblets, it is certainly not limited to this function. Any surface which can be molded into or otherwise represented on PVC adhesive film (and is not affected by prolonged contact with water) can be tested for drag properties.

These may include turbulence-promoting profiles (e.g. golf ball dimples), surface treatments (e.g. Teflon coatings), and even water-proof paints. It is not limited to testing just surfaces either, as it would be possible to study the drag reducing behavior of solution containing dilute concentrations of polymers or surfactants, which will be the subject of future investigations involving the instrument.

References

Bechert DW; Bruse M; Hage W; Van der Hoeven JGT; Hoppe G (1997) Experiments on drag-reducing surfaces and their optimization with an adjustable geometry. J Fluid Mech 338: 59–87

Joseph DD (1964) Variable viscosity effects on the flow and stability of flow in channels and pipes. Phys Fluids 7: 1761–1771

Joseph DD (1965) Stability of frictionally-heated flow. Phys Fluids 8: 2195–2200

Kreith F (1968) Convective heat transfer in rotating systems. Adv Heat Transfer 5: 129–251

Taylor GI (1936) Fluid friction between rotating cylinders I – Torque measurements. Proc Roy Soc A 223: 546–564

Walsh MJ (1990) Riblets. In: Bushnell DM; Hafner JN (eds.) Viscous Drag Reduction in Boundary Layers. Progress in Astronautics and Aeronautics, Vol. 123, pp. 203–261, Washington, DC: American Institute of Aeronautics and Astronautics, Inc.